Atmos. Chem. Phys. Discuss., https://doi.org/10.5194/acp-2017-1046
Manuscript under review for journal Atmos. Chem. Phys.
Discussion started: 13 December 2017

Atmospheric Chemistry and Physics
Discussions

Influence of boundary layer structure on air quality in Beijing: Long-term analysis based on self-organizing maps

Zhiheng Liao[a], Jiaren Sun[a, b]*, Jialin Yao[c], Li Liu[a], Haowen Li[a], Jian Liu[a], Jielan Xie[a], Dui Wu[d], Shaojia Fan[a]*

[a] School of Atmospheric Sciences, Sun Yat-sen University, Guangzhou, Guangdong, China;

[b] South China Institute of Environmental Sciences, Ministry of Environmental Protection of the People's Republic of China, Guangzhou, Guangdong, China;

[c] Weather Modification Office of Shanxi Province, Taiyuan, Shanxi, China;

[d] Institute of Mass Spectrometer and Atmospheric Environment, Jinan University, Guangzhou, Guangdong, China.

* Address correspondence to S. Fan or J. Sun, School of Atmospheric Sciences, Sun Yat-sen University, Guangzhou, Guangdong, China. Telephone: +86 020 8411 5522.

E-mail: eesfsj@mail.sysu.edu.cn (S. Fan); sunjiaren@scies.org (J. Sun).

Abstract

Self-organizing maps (SOMs; a feather-extracting technique based on an unsupervised machine learning algorithm) are used to classify the atmospheric boundary layer (ABL) types over Beijing by detecting topological relationships among the 4-yr (2013–2016) radiosonde profiles. The resulting ABL types are then examined in relation to air quality, including surface pollutant concentrations and columnar aerosol properties, to understand the regulating effects of different ABL structures on Beijing's air quality. The SOM provides nine ABL types (i.e., SOM nodes), and each type is characterized by distinct dynamic and thermodynamic conditions. On average, SO_2, NO_2, CO, PM_{10} and $PM_{2.5}$ increase 120–220 % from a near neutral (i.e., node 1) to strong stable condition (i.e., node 9). The ABL controls on diurnal cycles of pollutants are as follows: (1) elevated inversion enhances the afternoon baseline; and (2) surface inversion improves the evening increment. Comparing the CO/SO_2 ratios for the different ABL types demonstrates that the local contribution increases with enhanced static stability near the ground, and it is the stable ABL stratification rather than weak surface wind that confines the regional contribution. Due to regional transport, node 3 (dominated by elevated inversion with high relative humidity) corresponds to the most severe columnar aerosol pollution, characterized by the highest optical depth (1.22) and volume concentration (0.30 $\mu m^3/\mu m^2$). The larger aerosol radiative forcing (ARF) within the atmosphere (> 60 W/m^2) in nodes 3, 6 and 9 is likely to strengthen the atmospheric stability and thus induce a positive feedback loop for

causing high surface pollution. Analysis of the typical pollution period suggests that the ABL types are the primary drivers of day-to-day variations in Beijing's air quality. Assuming a fixed relationship between ABL type and $PM_{2.5}$ loading for different years, the relative (absolute) contribution of the ABL anomaly to elevated $PM_{2.5}$ levels are estimated to be 65.8 % (46.2 μg/m^3) during January 2013, 46.7 % (20.2 μg/m^3) during December 2015, and 94.6 % (35.3 μg/m^3) during December 2016.

1 Introduction

The atmospheric boundary layer (ABL) is the section of atmosphere that responds directly to the flows of mass, energy and momentum from the earth's surface, characteristically at timescales of an hour or less (Stull, 1988). Most air pollutants are emitted or chemically produced within this layer and its evolution plays an important role in determining the dispersive and chemical properties of pollutants (Chen et al., 2012; Fan et al., 2008; Whiteman et al., 2014; Platis et al., 2016; Wolf et al., 2014; Wu et al., 2013). Therefore, characterizing typical ABL conditions associated with high pollution levels helps to better understand the role of ABL in governing the transport and distribution of pollutants in the atmosphere.

Beijing, the capital of China, is suffering serious air pollution problems. This city is geographically located at the northwestern border of the Great North China Plain and has three directions that are adjacent to mountains. The closest coast from the city of Beijing is the Bohai Sea, which is 160 km southeast of the city. Terrain-related circulations can therefore be well developed over Beijing and its surroundings under favorable weather conditions, leading to a complex ABL thermodynamic structure, which is thought to substantially affect Beijing's air quality (Hu et al., 2014; Miao et al., 2017; Ye et al., 2016; Gao et al., 2016; Xu et al., 2016). Several studies used tower-based observations to investigate the interactions between boundary layer dynamics and pollution formation (Sun et al., 2013; Sun et al., 2015; Guinot et al., 2006). However, the results are not ideal because they have a low observational height (325 m). Numerous intensive ABL measures were conducted using other approaches, such as mooring boats, airplane, and ground remote sensing (Tang et al., 2015; Zhu et al., 2016; Zhang et al., 2009; Hua et al., 2016). However, since these approaches are complex, expensive and labor intensive, they are often restricted to the duration of specific research campaigns. Overall, the existing knowledge of linkages between ABL structure and air quality in Beijing is drawn largely from either low observational height or short observational duration. Due to the lack of long-term effective observations, the influence of ABL on Beijing's air quality remains relatively unclear. For example, many case studies (Jia et al., 2008; Zheng et al., 2015; Hua et al., 2016; Li et al., 2016) claimed that rapid growth of $PM_{2.5}$ in Beijing is mainly attributable to the regional transport of the polluted air mass. This view is occasionally questionable, as it is known that the polluted episodes tend to occur with a weak surface wind and stable boundary layer stratification, which are unfavorable for transport (Zhu et al., 2016; Tang et al., 2015). Given these uncertainties, there is an urgent need to investigate and determine the common patterns of ABL structure influence on Beijing's air quality.

On the other hand, the long-term radiosondes are not being fully utilized to investigate urban pollution issues. The advantage of radiosondes over the other approaches seems to be their length, which usually spans several decades. For a long time, it was challenging to reduce the wealth of radiosonde datasets to characterize the ABL structure, therefore, radiosondes remain in very limited use in case studies (Ji et al., 2012; Zhao et al., 2013; Gao et al., 2016). Recently, self-organizing maps (SOMs; a feather-extracting technique based on an unsupervised machine learning algorithm) (Kohonen, 2001) were introduced to investigate the ABL thermodynamic structure, indicating the capabilities of SOMs in feather extraction from a large dataset of the ABL measurements (Katurji et al., 2015). In fact, the SOM has become increasingly popular in atmospheric and environmental sciences during the past several years (Jensen et al., 2012; Jiang et al., 2017; Gibson et al., 2016; Pearce et al., 2014; Stauffer et al., 2016), including a first application of routine radiosondes in South Africa (Dyson, 2015). However, there is thus far no SOM application in pollution-related ABL structure research. It is expected that such a new analytical approach can tap the potential of routine radiosondes to better understand urban air pollution.

In this study, a long-term analysis regarding the influence of ABL structure on Beijing's air quality is performed based on the application of SOMs to 4 years (2013-2016) of radiosonde measurements. The SOM is first used to classify the vertical temperature profiles for identifying predominant ABL types (see section 3.1). A selection of climatological observations is then subdivided according to the SOM-based ABL classification (see section 3.2). Finally, we provide a visual insight into air quality variations (including surface pollutant concentrations and columnar aerosol properties) under various ABL conditions and discuss the potential physical mechanisms behind their relationships (see section 3.3–3.5). It is expected that such an association between air quality and ABL type could provide local policy makers with useful information for improving the predictions of urban air quality.

2 Materials and methods

2.1 Data preparation and preprocessing

Radiosonde data observed at the Beijing Observatory (39.81°N, 116.48°E, WMO station number 54511) were collected from the University of Wyoming (http://weather.uwyo.edu/). The data cover the recent 4-year period

Atmos. Chem. Phys. Discuss., https://doi.org/10.5194/acp-2017-1046
Manuscript under review for journal Atmos. Chem. Phys.
Discussion started: 13 December 2017

from 2013 to 2016. The Beijing Observatory launches a routine radiosonde twice a day (08:00 and 20:00 Beijing Time (BJT), corresponding to the morning and evening, respectively) and provides atmospheric sounding data (profiles of temperature, relative humidity, wind speed, etc.) at the mandatory pressure levels (e.g., surface, 1000, 925, 850, 700 hPa) and additional significant levels. In addition, the hourly near-surface meteorological parameters (including temperature, wind speed and relative humidity) are also collected from the Beijing Meteorological Bureau.

We chose the 2000 m above ground level (AGL) as the upper limit of the ABL based on a number studies investigating the ABL height over Beijing or North China (Tang et al., 2016; Guo et al., 2016; Miao et al., 2017). This height exceeds the ABL height in most cases, and therefore, most ABL processes influencing the near-surface air quality are included in the analysis herein. We classify the daily ABL types using the SOM algorithm. To keep a whole night, the daily vertical profiles are composited from the radiosonde measurements at 20:00 and 08:00 of the next day.

The mass concentrations of atmospheric pollutants (including SO_2, NO_2, CO, O_3, PM_{10} and $PM_{2.5}$) over Beijing during the period from 2013 to 2016 are obtained from the Ministry of Environmental Protection of the People's Republic of China (http://datacenter.mep.gov.cn/). In addition, hourly $PM_{2.5}$ measured at the Beijing US Embassy (http://www.stateair.net/) are also used in this study. Hourly concentrations are calculated for the Beijing urban area by averaging concentrations from nine urban sites (including Dongsi, Guanyuan, Tiantan, Wanshouxigong, Aotizhongxin, Nongzhanguan, Gucheng, Haidianwanliu and US Embassy). To maintain consistency with ABL classification, the daily pollutant concentration is performed from noon-to-noon (12:00 h–12:00 h).

In addition to near-surface observations, columnar aerosol parameters (including aerosol optical depth (AOD), Ångström exponent (AE), single scattering albedo (SSA), volume particle size distribution (d*V*/dln*R*), aerosol radiative forcing (ARF) and so on) are also collected from the AERONET Beijing (39.98°N, 116.38°E) and Beijing-CAMS (39.93°N, 116.32°E) sites. The level-2.0 quality-assured columnar aerosol data from 2013 to 2016 are downloaded from the AERONET data archive (http://aeronet.gsfc.nana.gov). The size distribution is retrieved in 22 logarithmically equidistant bins in a range of sizes from 0.05 to 15 μm through a combined spherical and spheroid particle model (Dubovik and King, 2000; Dubovik et al., 2006).

2.2 Self-organizing maps technique

The SOM is an ideal tool for feather extraction because the input data are treated as a continuum without relying on correlation, cluster or eigenfunction analysis (Liu et al., 2006). Since Kohonen (1982) first proposed SOM, it has been widely used for data downscaling and visualization in various disciplines (Jensen et al., 2012; Katurji et al., 2015; Dyson, 2015; Stauffer et al., 2016; Pearce et al., 2014; Jiang et al., 2017). In this study, the SOM is introduced to classify the ABL structures. We use the code from the MATLAB SOM Toolbox, which is freely available from http://www.cis.hut.fi/projects/somtoolbox/.

The following provides a simple introduction about the SOM algorithm, and the details can be found in Kohonen (2001). SOM training is an unsupervised, iterative procedure, and the result is a matrix of nodes (i.e., types) that represent the input data. To learn from the input data, every SOM node has a parametric reference vector with which it is associated, and these reference vectors are randomly generated. After initialization of the reference vectors, a stochastic input vector is compared to every reference vector, and the closest match, named the best-matching unit, is determined by the smallest Euclidean distance. Each reference vector is then updated so that the best-matching unit and its neighbors become more like the input vector. Whether or not a reference vector learns from the input vector is determined by the neighborhood function. Only reference vectors that are topologically close enough to the best-matching unit will be updated according to the SOM learning algorithm.

To exclude the influence of actual temperature values, temperature deviation profiles, which are determined by subtracting the mean temperature of each profile from each level in the profile, are used as the SOM input in this study. The first step of SOM training is to determine a matrix size of nodes for initializing the reference vectors. This step is performed subjectively and depends on the degree of generation required (Lennard and Hegerl, 2015). We test several SOM matrixes and finally select a 3×3 matrix, because it captured unique profiles without the profiles being too general as with a smaller matrix or being too similar as with a larger matrix. The batch mode is chosen to execute the SOM algorithm. This mode is much more computationally efficient compared to the sequence mode. The other user-defined settings in the SOM software are set at the default, such as the hexagon topology, Gaussian neighborhood function, etc.

3 Results and discussion

3.1 Self-organized ABL types

We constructed a 3×3 SOM matrix for daily temperature deviation profiles, and the SOM output shown in Fig. 1 represents nine ABL types (i.e., SOM nodes). In Fig. 1, the SOM nodes are plotted in red, and the individual profiles corresponding to the SOM node are plotted in blue. For comparison, the mean and 25th and 75th percentiles for the entire period are plotted in cyan. On the SOM plane, the most notable feather is adjacency of like types (e.g., nodes 1 and 2) and the separation of contrasting types (e.g., nodes 1 and 9). Although the SOM nodes appear to be sorted in a certain order, there is no physical significance associated with this order. Such ordering is a feather of the SOM algorithm (i.e., 'self-organized'). This feather allows us to visualize subtle differences between the neighboring clusters of profiles and distinguish the unique characteristics of nodes through the variation of specific features across the SOM plane.

The SOM classification reveals that for the whole study period, the ABL is dominated by near neutral to strong stable conditions, as none of the SOM nodes fall within the unstable category (i.e., super-adiabatic condition). The results are reasonable, considering the daily temperature profile is composited from 20:00 and 08:00 measurements. According to the SOM ordering feather, the SOM nodes in four corners (i.e., nodes 1, 3, 7 and 9) can be thought of as the typical ABL types and the others can be considered transitional ABL types. It is clear from the individual profiles in Fig. 1 that node 1 represents the well-mixed (near-neutral) condition with no temperature inversion, node 3 indicates the ABL type dominated by elevated inversion, node 7 indicates the ABL type dominated by surface inversion, and node 9 represents the ABL type associated with multiple inversions (i.e., including surface and elevated inversions).

Frequency analysis of the nine ABL types indicates that the frequency distribution across the types is quite varied from the expected 11.1 %, with the occurrence frequency showing a 5:1 range from the most frequent type (node 1) to the least frequent type (node 5). The higher-frequency types are presented on the outer portions of the SOM plane, while lesser-frequency types are presented closer towards the center (top-right in Fig. 1). The most dominant types are nodes 1 and 3, and their occurrence frequencies reach 22 % and 20 %, respectively. As synoptic circulations change with the seasons over Beijing, the ABL types are expected to correspond to seasonality. The number of profiles from each season in each ABL type is expressed as a percentage and is shown in Fig. 2. All of the types exhibit strong seasonality. For example, node 1 has the highest occurrence in spring (29.4 %) and the lowest occurrence in autumn (13.7 %); node 9 presents the highest occurrence in winter (16.3 %) and the lowest occurrence in summer (4.9 %).

3.2 Evaluation against meteorological data

Fig. 3 shows the average vertical profiles of potential temperature, wind speed and relative humidity corresponding to each ABL type. As seen in Fig. 3, each of the ABL types is associated with distinct dynamic and thermodynamic conditions. The potential temperature profiles vary from near neutral conditions to strong stable conditions, and this change is closely related to the variance in wind speed, suggesting a strong coupling between the dynamic and thermal effects. The two extreme types (nodes 1 and 9) provide a very useful example. Node 9 is a very strong stable profile, and the wind speeds are very low in the lower ABL. In contrast, node 1 is a well-mixed (near neutral) profile and it corresponds to significantly higher wind speeds throughout the ABL. In addition, when the stability of the atmosphere is strong, vertical mixing is suppressed and winds in the lower ABL become decoupled from the generally stronger wind aloft. This allows moisture, fogs, low clouds and other scalars to build up within the stable layer. As a result, the stable ABL types usually correspond to high RH in the lower ABL.

The near-surface meteorological variables are also examined for each of the ABL types. Fig. 4 shows the diurnal composite plots of surface temperature, wind speed and relative humidity in the four typical ABL types. As expected, these near-surface variables respond well to the changing ABL structure. Wind speeds are the highest on the days corresponding to near neutral conditions (i.e., node 1). High wind speeds result in a deep, mechanically mixed layer, and these days also exhibited the smallest diurnal amplitude in wind speed, temperature and relative humidity. Such characteristics are likely consistent with the passage of frontal systems. In contrast, the smallest wind speeds are observed on days related to strong stable conditions (i.e., node 9). The stable days also generally exhibit the greatest amplitude of the diurnal signals in temperature and relative humidity. This fact is an indication that stable conditions occur mostly on clear sky days.

3.3 Evaluation against surface air quality

The concentrations of gaseous and particulate pollutants in the atmosphere are governed by the rate at which they are emitted from their respective sources, lost by various sink mechanisms, and characteristics of the atmospheric volume into which they mix. While the mixing volume is determined primarily by the boundary layer structure, the chemical transformation also depends on boundary layer meteorology in some cases. In the previous section, it was seen that the SOM technique is an effective tool for classifying boundary layer structures. In this section, we used the classification technique to quantify the influence of the boundary layer structure on near-surface air quality.

Fig. 5 examines the daily concentrations of gaseous and particulate pollutants in relation to various ABL types.

As expected, the most stable conditions are associated with a dramatic increase in the mass concentrations of air pollutants (except O_3). On average, SO_2, NO_2, CO, PM_{10} and $PM_{2.5}$ increase by 15.7 μg/m^3 (142 %), 44.3 μg/m^3 (119 %), 1.5 mg/m^3 (202 %), 91.6 μg/m^3 (119 %) and 95.9 μg/m^3 (218 %) from the near neutral ABL condition (i.e., node 1) to strong stable condition (i.e., node 9), respectively. The highest increasing amplitude is related to $PM_{2.5}$, suggesting fine particulate matters are likely accumulated from not only primary emissions but also secondary formation (Zhang and Cao, 2015). As we have shown, the more stable ABL conditions tend to correspond to high relative humidity in the lower ABL (Figs. 3 and 4). Additional enhancement in $PM_{2.5}$ can be expected under the humid condition, as it is known that the humidity-related physicochemical formation of particles (such as hygroscopic growth, liquid-phase and heterogeneous reactions) can be intensified by high humidity values (Cheng et al., 2015; Cheng et al., 2016; Zheng et al., 2015).

Interestingly, increasing atmospheric stability has an opposite effect on near-surface O_3 concentrations. Since O_3 is produced by photochemical interactions between NO_x (NO + NO_2) and volatile organic compounds (VOCs) (Seinfeld and Pandis, 2006), the boundary layer structure alters the O_3 level through modulation of its precursors (NO_x and VOCs). The low O_3 level in the stable ABL can be explained by the strong titration reaction. Since O_3 is highly reactive, when trapped in a stable layer, surface titration by the NO emitted from vehicles can cause a rapid reduction in O_3 concentration. In previous studies, persistent low O_3 concentration were observed in the stable boundary layer condition in Beijing (Zhao et al., 2013). Conversely, when near-surface wind speeds are higher (near neutral condition such as node 1), O_3 is mixed downward from the overlying air mass, resulting in higher concentrations. Nevertheless, it is worth noting that the extremely high O_3 values (not shown) were also detected on very stable days (i.e., node 9), suggesting the complexity of O_3 behavior in response to the boundary layer structure (Tong et al., 2011; Haman et al., 2014).

To obtain a more in-depth understanding of the physical mechanisms behind the relationship between air quality and ABL structure, diurnal composite hourly concentrations of atmospheric pollutants are formed for each ABL type. The SOM-based ABL classification scheme provides a consistent, gradual distinction in the diurnal cycles of surface air pollutants from near neutral to strong stable conditions. The composite diurnal evolutions of air pollutants in the four typical ABL types (i.e., nodes 1, 3, 7 and 9) are illustrated in Fig. 6. The diurnal cycles of SO_2, NO_2, CO, PM_{10} and $PM_{2.5}$ are extremely pronounced under the strong stable condition (i.e., node 9), although very reduced under the near neutral condition (i.e., node 1). In contrast, the behavior of O_3 is completely different from other pollutants. The results suggest that the chemical species, which are mainly produced by surface emissions, are strongly modulated by the development of the ABL, while the chemical species, which are strongly controlled by the photochemical process, are weakly regulated by the development of the ABL (Crawford et al., 2016). Overall, the diurnal behavior of each pollutant species in each of the ABL types is generally consistent with the existing knowledge for urban areas (Chambers et al., 2015b; Chambers et al., 2015a; Zhang et al., 2012b; Jenner and Abiodun, 2013; Han et al., 2009).

Of particular interest in Fig. 6 is that (1) nodes 3 and 9 have similar magnitudes of concentrations in the afternoon, and (2) nodes 7 and 9 have similar increments in concentrations from afternoon to midnight, although there is a huge distinction in the afternoon concentrations (i.e., afternoon baselines). This sheds some light on the common patterns of the ABL controls on the near-surface air quality in Beijing. Considering the thermal inversion feather in each of ABL types (Fig. 1), the regulating effects of ABL on near-surface concentrations can be concluded as follows: (1) elevated inversion enhances the afternoon baseline; and (2) surface inversion improves the evening increment. Obviously, the high afternoon baselines in nodes 3 and 9 can be attributed to elevated inversion, while high evening increments in nodes 7 and 9 can be attributed to surface inversion. Since surface inversion usually develops shortly before sunset due to radiation cooling, the evening traffic emission peak is counteracted by a stabilizing boundary layer. Consequently, the air pollutants such as NO_2, CO, PM_{10} and $PM_{2.5}$ often experience an explosive growth from afternoon to midnight. In contrast, elevated inversion usually forms due to synoptic forcing (such as synoptic advection) (Hu et al., 2014; Xu et al., 2016) and can persist for several days; as a result, the daytime mixing volume is also depressed, causing a relatively higher afternoon concentration.

Beijing has relatively little industry but numerous automobiles, and the emissions of SO_2 are small while those of CO, NO_x and particles are much larger (Zhao et al., 2012). By comparison, the diurnal behaviors of SO_2 and other pollutants are completely different. For example, in node 9, SO_2 show a lower nighttime concentration but a sharp increase after sunrise, whereas NO_2, PM_{10} and $PM_{2.5}$ show a higher nighttime concentration with a slight morning increase associated with the traffic emission. The results largely suggest that the changing ABL structure affects the near-surface observations of locally and remotely sourced pollutants in very different ways. In the evening, since the stable boundary layer (SBL) and the residual layer (RL) are essentially decoupled with each other (Stull, 1988), locally sourced pollutants emitted into the surface layer (such as CO, NO_2 and particulate matters from vehicular emissions) become trapped close to the surface. In contrast, remotely sourced pollutants emitted from chimneystacks above the SBL (such as SO_2 from power plants in the Hebei Province) may be stored

Atmos. Chem. Phys. Discuss., https://doi.org/10.5194/acp-2017-1046
Manuscript under review for journal Atmos. Chem. Phys.
Discussion started: 13 December 2017

within the RL aloft and not penetrate into the SBL. As the daytime convective turbulent mixing developed in the morning, the rapid momentum transfer between the surface and aloft air transported the pollutants stored in RL downward and meanwhile upwardly mixed the pollutants trapped from the previous night in the surface layer (Salmond and McKendry, 2005). It is observed in Fig. 6 that after a stable night, the burst of turbulent activity in the morning coincides with a rapid increase in SO_2 concentration (Fig. 6). Since there is no significant increase in SO_2 emission at the surface at this time, this result strongly suggests that increased SO_2 in the morning resulted from the downward mixing of stored SO_2 in the RL aloft. In a previous case study, Li et al. (2017b) reported that as a result of both turbulent mixing and the advection of high concentrations of air pollutants above the surface layer, the urban area of Beijing experienced a dramatic increase of the $PM_{2.5}$ concentration in the morning on 30 November 2015.

Given the importance of local vehicle emissions vs. more-distance power plant and industrial emissions for Beijing's air quality, the ratio of CO/SO_2 can be considered as an indicator of the contribution of local emissions to air pollution, with higher ratios indicating higher local contributions (Tang et al., 2015). Fig. 7 shows the composite diurnal variations of CO/SO_2 ratios in the four typical ABL types (i.e., nodes 1, 3, 7 and 9). The contrasts between CO/SO_2 ratios for the various ABL types are noticeable during the nighttime, whereas differences during the daytime are minimal. During the daytime, when the ABL is well mixed, near-surface pollutant concentrations represent a combination of local and remote sources. In the evening, however, the earth's surface begins to cool, and a stable boundary layer begins to form from the ground up. If sufficiently strong, the nocturnal surface inversion can isolate near-surface observations from the influence of distant sources (Crawford et al., 2016). Consequently, the more stable the nocturnal conditions near the ground, the higher the CO/SO_2 ratios that occur (Fig. 7). The results are consistent with previous studies (Tang et al., 2015; Zhu et al., 2016), indicating local contribution increases with enhanced static stability in the surface layer over Beijing. According to the above analysis, high pollutant loadings in node 9 are mostly attributable to local contributions (the highest CO/SO_2 ratios in node 9); however, high pollutant loadings in node 3 are more likely due to regional contributions (the lowest CO/SO_2 ratios in node 3). Obviously, it is the stable stratification rather than the weak surface wind that confines the regional contribution.

3.4 Evaluation against columnar aerosol pollution

For many years, aerosol particles have been the primary pollution problem in Beijing. Atmospheric aerosols play an important role in radiation transfer due to absorption and/or scattering in the atmosphere, and thus could have a great influence on the evolution of the ABL. In recent years, the feedback effect of aerosols on the ABL has drawn much attention (Kajino et al., 2017; Gao et al., 2016; Ding et al., 2016). To further our understanding of aerosol pollution in Beijing, we examine the optical and physical properties and the direct radiative forcing of columnar aerosols in the different ABL types in this section.

Aerosol optical properties can be characterized by three useful parameters: AOD, AE and SSA. Fig. 8 illustrates the AOD_{440nm}, $AE_{440nm-870nm}$ and SSA_{440nm} over Beijing within the nine ABL types. The ABL-type averages of AOD range from 0.52 and 1.22 (Fig. 8a). Comparing with near-surface observations, the greatest difference is that the highest AOD value generally occurs in node 3, rather than in node 9 (the highest surface $PM_{2.5}$ and PM_{10} concentrations occur in node 9). This may be attributed to the difference in aerosol vertical distribution in these two types. As we have demonstrated in Sect 3.3, node 3 is related to strong regional transport. Since the height of regional transport is usually above the surface layer, such as 200–700 m AGL detected by Li et al. (2017a), more aerosol particles might be suspended above the surface layer in node 3, resulting in the highest AOD value in the atmospheric column. In addition, since high relative humidity also occurs in node 3, the highest AOD value in this ABL type could be partly attributed to the particle hygroscopic growth (Chen et al., 2014; Deng et al., 2016; Zhao et al., 2017).

It is known that high AE values indicate a dominance of fine particles, while low values indicate a dominance of coarse particles. Unlike AOD, the AE shows a relatively low sensitivity to ABL types (Fig. 8b). All type averages of AE are higher than 1.0, suggesting that the proportion of fine particles is always larger than that of coarse particles over Beijing (Yu et al., 2017; Yu et al., 2009). The highest AE occurs in node 6 (1.20) and the lowest is 1.03 in node 1. Node 1 corresponds to the lowest AE value, indicating that under the near neutral ABL condition, the coarse particles contribute a relatively higher proportion of total particles. This could be due to the increasing wind speed with decreasing relative humidity (Figs. 3 and 4). Coarse particles could be from more natural and anthropogenic dust emission under high wind speed conditions. Particularly during the fast northwesterly wind period, dust storms occasionally contribute to the high coarse particle loadings in Beijing (Yu et al., 2016). The long-distance transport of dust particles from northwest China may be the reason for the lowest AE value in node 1.

The SSA is defined as the ratio of the scattering coefficient and the total extinction coefficient. It is mostly dependent on the aerosol size, concentration of absorbing component and its mixture state with non-absorbing

Atmos. Chem. Phys. Discuss., https://doi.org/10.5194/acp-2017-1046
Manuscript under review for journal Atmos. Chem. Phys.
Discussion started: 13 December 2017

components. The daily SSA at 440 nm ranges from 0.82 to 0.98 during the study period, which suggests that there are quite different types of aerosols in the columnar atmosphere over Beijing (varying from strong absorbing aerosols to strong scattering aerosols). It is easy to see that the ABL types associated with a strong surface inversion (i.e., nodes 7, 8 and 9) have lower SSA values (Fig. 8c). The averaged SSA in these nodes is approximately 0.90, which is significantly lower than that in nodes 1, 2 and 3. The low SSA values mean enhancement in the absorbing particles, such as black carbon, which are released from industry, biomass/biofuel burning, diesel vehicle, and coal burning. In contrast, the highest SSA occurring in node 1 can be explained by dust particle transmission and soil aerosol emissions.

The volume particle size distribution retrieved in the sizes between 0.05 and 15 μm is one of the most important parameters for studying the behavior of aerosols (Dubovik and King, 2000). Fig. 9 expresses the mean volume particle size distribution (d*V*/dln*R*) over Beijing in the nine ABL types. Table 1 supplements Fig. 9 with the statistical parameters of aerosol particle size distribution. Clearly, the volume particle size agrees very well with the bimodal lognormal distributions. Both fine (R < 0.6 μm) and coarse (R > 0.6 μm) modes exhibit relative stability with two peaks at a radius of approximately 0.1–0.2 μm and 2.0–4.0 μm, which are similar to some previous studies (Eck et al., 2005; Xia et al., 2007; Che et al., 2014). However, the size distribution shows a distinct difference in the changing amplitude for different ABL types. The fine- and coarse-mode particle volumes increase rapidly from left (nodes 1, 4 and 7) to right (nodes 3, 6 and 9) on the SOM plane. This suggests that with the stabilizing boundary layer processes, the atmosphere is more loaded with both fine- and coarse-mode particles over Beijing. In addition, the stabilizing processes are accompanied by the increase of the fine-mode effective radius (R_{eff}-F) and fine-mode volume fraction (Vf/Vt). These results strongly point to the important role of fine-mode particle hygroscopic growth on the days associated with stable nocturnal ABL conditions.

The type-averaged ARF at the surface (BOA), top of atmosphere (TOA), and within the atmosphere (ATM) over Beijing is shown in Fig. 10. The type averages of ARF at the surface range from -47.8 W/m^2 to -110.0 W/m^2, while at the TOA, they are found to be between -21.1 W/m^2 and -48.0 W/m^2. Likewise, the ABL type averaged ARF within the atmosphere are between 26.7 W/m^2 and 63.1 W/m^2. The larger negative ARF at the surface (> 110 W/m^2) and positive ARF within the atmosphere (> 60 W/m^2) are found in ABL types 3, 6 and 9 over Beijing, implying strong cooling at the surface and warming in the atmosphere. These results are induced by relatively larger aerosol loadings under the stagnant meteorological conditions. The larger ARF within the atmosphere demonstrates that solar radiation is being absorbed within the atmosphere, and as a result, heats the atmosphere and reduces surface temperature. This can change the atmospheric vertical temperature gradient and improve the atmospheric stability (Li et al., 2010; Ge et al., 2010; Zou et al., 2017). Finally, the enhanced stability hinders the vertical diffusion of aerosol particles, leading to the increase of aerosol concentrations and causing a further decrease in the solar radiation and ABL height, which induces a positive feedback loop for causing high surface aerosol concentrations (Quan et al., 2013; Zhong et al., 2017).

3.5 Evaluation against heavy polluted episodes

In January of 2013, December of 2015, and December of 2016, heavy aerosol pollution episodes frequently wreaked havoc across Beijing and its surroundings, which resulted in severe damages to the environment and human health. Fig. 11 shows the hourly variations of $PM_{2.5}$ and AOD_{440nm} during the three heavily polluted months. It is observed that the $PM_{2.5}$ concentrations were frequently elevated to above 200 μg/m^3, and the AOD often exceeded 1.0 in Beijing during these three months. The ABL types (shown at the top of each plot) reveal that pollution episodes were generally associated with the control of nodes 3 and 9, and clean episodes were often associated with the control of node 1. For example, the severe pollution episode that occurred from 9–14 January 2013 was due to the alternate control of nodes 3 and 9, and the pollution episode from 15–21 December 2016 was related to the persistent control of node 9. In contrast, multiday control of node 1 caused a clean episode from 14–16 December 2015. The linkages between air quality and the boundary layer structure were consistent with the long-term analyses described in Sects. 3.3 and 3.4, indicating that the ABL types are one of the primary drivers of day-to-day variations in air quality over Beijing.

The monthly $PM_{2.5}$ concentrations in the Beijing urban area reached up to 180.8 μg/m^3, 153.9 μg/m^3 and 147.9 μg/m^3 in January 2013, December 2015 and December 2016, respectively. All these values were far larger than the 4-yr winter mean $PM_{2.5}$ concentration (110.6 μg/m^3). Although the characteristics of $PM_{2.5}$ air quality depend on many complex elements, the major contributors are the pollutant emissions and meteorological conditions. In 2013, the Chinese State Council released the “Atmospheric Pollution Prevention and Control Action Plan” to implement a megacity cluster-scale joint prevention and control strategy program. As a result, the $PM_{2.5}$ in Beijing decreased from 89.5 μg/m^3 in 2013 to 73.0 μg/m^3 in 2016. However, these meteorology-driven pollution episodes to some degree obscure the true impacts of the emission control strategies implemented by government. Fig. 12 shows a comparison of the occurrence frequency of the nine ABL types to the winter mean frequency (2013-2016) for the three polluted months. Compared with the 4-yr winter mean frequency, the greatest differences are that the occurrences of nodes 3 and 9 (the two most polluted types) increased and node 1 (the clean type) decreased during the three polluted months. Obviously, the elevated $PM_{2.5}$ concentrations in the abovementioned months can be mostly attributable to the anomalous boundary layer structures.

Quantitative analysis of the roles of the ABL anomaly in $PM_{2.5}$ variations during the pollution months is helpful for the assessment of air pollution prevention and control strategies. In this study, the ABL classification allows for the integrated evaluation of the effects of numerous interrelated ABL meteorological parameters on air quality. Here, a meteorology-to-environment method (revised from the circulation-to-environment method proposed by Zhang et al. (2012a)) is utilized to evaluate the influence of the ABL anomaly for enhanced $PM_{2.5}$ levels during the abovementioned months. We assume the linkages between ABL types and their $PM_{2.5}$ loadings in winter are constant in different years. For each polluted month, the total anomaly (C') is defined as the deviation in $PM_{2.5}$ from the 4-yr winter mean concentration ($\overline{C}$). This total anomaly in each month is due to the combined effects of meteorology and emission. The anomaly calculated from the mean $PM_{2.5}$ loadings for nine ABL types and their occurrence frequencies during each month can be considered to represent the $PM_{2.5}$ change caused by the anomalous boundary layer structure. We refer to this as the "ABL-driven" anomaly. The ABL-driven anomaly (C_{ABL}') is calculated through $\sum_i F_i \cdot C_i - \overline{C}$, where F_i is the occurrence frequency of type-i ABL during a specific period and C_i is the corresponding $PM_{2.5}$ loading feathering that type. The ratio of C_{ABL}' to C' (the difference of C_{ABL}' to $\overline{C}$) is then used to evaluate the relative (absolute) contribution of the ABL anomaly to the enhanced $PM_{2.5}$ level. The results show that the contributions of the frequency anomaly of the ABL type to the increase in $PM_{2.5}$ are 65.8 % (46.2 μg/m^3) during January 2013, 46.7 % (20.2 μg/m^3) during December 2015 and 94.6 % (35.3 μg/m^3) during December 2016. These quantitative estimations suggest that the ABL anomaly to a large extent explains the enhanced $PM_{2.5}$ concentrations during these polluted months.

4. Summary

The influence of the ABL structure on Beijing's air quality is still unclear due to the lack of long-term observations. On the other hand, the long years of routine radiosondes remain underutilized as a tool for urban pollution studies. In this study, the SOM was applied to 4-yr radiosondes to classify the ABL types over Beijing. The resulting types were then evaluated in relation to meteorological and environmental variables, with an attempt to understand the roles of different ABL conditions in regulating the air quality in Beijing. The main findings are as follows:

1) The SOM provides a continuum of nine ABL types (i.e., SOM nodes), and each type is characterized with

distinct boundary layer meteorological conditions (including dynamic and thermodynamic conditions).

2) From the near neutral (i.e., node 1) to strong stable ABL types (i.e., node 9), the surface concentrations of SO_2, NO_2, CO, PM_{10} and $PM_{2.5}$ on average increase approximately 120–220 %. The diurnal evolutions of these pollutants are strongly modulated by temperature inversions. While an elevated inversion enhances the afternoon baseline concentration, the surface inversion improves the evening concentration increment. In contrast, O_3 show an opposite variation in response to the ABL types.
3) Boundary layer evolution affects the near-surface observations of locally and remotely sourced pollutants in very different ways, causing a distinct difference in the diurnal variations of SO_2 and other pollutants (e.g., NO_2, CO, PM_{10} and $PM_{2.5}$). Comparing the CO/SO_2 ratios in different ABL types reveals that the local contribution increases with enhanced static stability near the ground, and it is the stable boundary layer stratification rather than weak surface wind that confines the regional contribution.
4) With the stabilizing ABL processes, the atmosphere column is more loaded with both fine- and coarse-mode particles. Node 3 (dominated by elevated inversion and high relative humidity) corresponds to the most severe columnar aerosol pollution, characterized by the highest optical depth (1.22) and volume concentration (0.30 $\mu m^3/\mu m^2$). The larger negative ARF at the surface (> 110 W/m^2) and positive ARF within the atmosphere (> 60 W/m^2) are associated with the three stable ABL types (i.e., nodes 3, 6 and 9), suggesting the possible influence of a positive feedback loop for causing high surface aerosol concentrations.
5) Analysis of three typical pollution months (i.e., January 2013, December 2015 and December 2016) suggests that the ABL types are one of the primary drivers of day-to-day variations in Beijing's air quality. During the three pollution months, the frequency of stable ABL types (e.g., nodes 3 and 9) increases significantly compared with the 4-yr (2013-2016) winter mean frequency. In contrast, the frequency of the well-mixed ABL type (i.e., node 1) is greatly reduced during these pollution months.
6) Using a meteorology-to-environment method, the relative (absolute) contribution of the ABL anomaly to enhanced $PM_{2.5}$ level is estimated to be 65.8 % (46.2 $\mu g/m^3$) during January 2013, 46.7 % (20.2 $\mu g/m^3$) during December 2015, and 94.6 % (35.3 $\mu g/m^3$) during December 2016.

This work revealed the common pattern of the influence of different ABL structures on Beijing' air quality. The established correlations between ABL type and air quality could be useful for developing an operational forecast and warning system. In addition, this work demonstrated that the SOM-based ABL classification scheme is a powerful tool for understanding urban air pollution. Since the SOM technique is good at feather extraction, the coarse-resolution radiosonde profiles can be taken as the SOM input (as we have shown in this study). Therefore, it can take advantage of the long-term available radiosondes, which is simple and economical to implement in comparison to conventional techniques (such as mooring boats, airplane, and ground remote sensing). We believe that the pollution-related ABL research and the formulation of pollution control measures could benefit from application of the SOM analytical tool.

Data availability

The datasets used in this study are publicly available at the University of Wyoming (http://weather.uwyo.edu/), the Ministry of Environmental Protection of the People's Republic of China (http://datacenter.mep.gov.cn/), the U.S. Department of State Air Quality Monitoring Program (http://www.stateair.net/), and the Aerosol Robotic Network (https://aeronet.gsfc.nasa.gov/).

Competing interests

The authors declare no conflict of interest.

Acknowledgements

This study is supported by the National Key Research and Development Plan of China (Nos. 2017YFC0209606 and 2016YFC0203305), the National Natural Science Foundation of China (Nos. 41630422, 41475140 and 41475004) and the Special Fund for Basic Scientific Research Business of Central Public Research Institutes (PM-zx703-201601-019). The authors would like to thank the Beijing Meteorological Bureau, the Ministry of Environmental Protection of the People's Republic of China and the Wyoming Weather Web for providing related data. Concerning the AERONET data used in this paper, we are particularly grateful to Prof. Huizheng Che, Prof. Hongbin Chen and Prof. Philippe Goloub for their efforts in establishing and maintaining the AERONET site in Beijing, as well as their assistants for the upkeep of the instrument and availability of the online data.

References

Chambers, S. D., Wang, F. J., Williams, A. G., Deng, X. D., Zhang, H., Lonati, G., Crawford, J., Griffiths, A. D., Ianniello, A., and Allegrini, I.: Quantifying the influences of atmospheric stability on air pollution in Lanzhou, China, using a radon-based stability monitor, Atmos Environ, 107, 233-243, 10.1016/j.atmosenv.2015.02.016, 2015a.

Chambers, S. D., Williams, A. G., Crawford, J., and Griffiths, A. D.: On the use of radon for quantifying the effects of atmospheric stability on urban emissions, Atmos Chem Phys, 15, 1175-1190, 10.5194/acp-15-1175-2015, 2015b.

Che, H., Xia, X., Zhu, J., Li, Z., Dubovik, O., Holben, B., Goloub, P., Chen, H., Estelles, V., Cuevas-Agullo, E., Blarel, L., Wang, H., Zhao, H., Zhang, X., Wang, Y., Sun, J., Tao, R., Zhang, X., and Shi, G.: Column aerosol optical properties and aerosol radiative forcing during a serious haze-fog month over North China Plain in 2013 based on ground-based sunphotometer measurements, Atmos Chem Phys, 14, 2125-2138, 10.5194/acp-14-2125-2014, 2014.

Atmos. Chem. Phys. Discuss., https://doi.org/10.5194/acp-2017-1046
Manuscript under review for journal Atmos. Chem. Phys.
Discussion started: 13 December 2017

Chen, J., Zhao, C. S., Ma, N., and Yan, P.: Aerosol hygroscopicity parameter derived from the light scattering enhancement factor measurements in the North China Plain, Atmos Chem Phys, 14, 8105-8118, 10.5194/acp-14-8105-2014, 2014.

Chen, L. W. A., Watson, J. G., Chow, J. C., Green, M. C., Inouye, D., and Dick, K.: Wintertime particulate pollution episodes in an urban valley of the Western US: a case study, Atmos Chem Phys, 12, 10051-10064, 10.5194/acp-12-10051-2012, 2012.

Cheng, Y., He, K. B., Du, Z. Y., Zheng, M., Duan, F. K., and Ma, Y. L.: Humidity plays an important role in the PM2.5 pollution in Beijing, Environ Pollut, 197, 68-75, 10.1016/j.envpol.2014.11.028, 2015.

Cheng, Y., Zheng, G., Wei, C., Mu, Q., Zheng, B., Wang, Z., Gao, M., Zhang, Q., He, K., Carmichael, G., Poschl, U., and Su, H.: Reactive nitrogen chemistry in aerosol water as a source of sulfate during haze events in China, Science advances, 2, e1601530, 10.1126/sciadv.1601530, 2016.

Crawford, J., Chambers, S., Cohen, D., Williams, A., Griffiths, A., and Stelcer, E.: Assessing the impact of atmospheric stability on locally and remotely sourced aerosols at Richmond, Australia, using Radon-222, Atmos Environ, 127, 107-117, 10.1016/j.atmosenv.2015.12.034, 2016.

Deng, H., Tan, H. B., Li, F., Cai, M. F., Chan, P. W., Xu, H. B., Huang, X. Y., and Wu, D.: Impact of relative humidity on visibility degradation during a haze event: A case study, Sci Total Environ, 569, 1149-1158, 10.1016/j.scitotenv.2016.06.190, 2016.

Ding, A. J., Huang, X., Nie, W., Sun, J. N., Kerminen, V. M., Petaja, T., Su, H., Cheng, Y. F., Yang, X. Q., Wang, M. H., Chi, X. G., Wang, J. P., Virkkula, A., Guo, W. D., Yuan, J., Wang, S. Y., Zhang, R. J., Wu, Y. F., Song, Y., Zhu, T., Zilitinkevich, S., Kulmala, M., and Fu, C. B.: Enhanced haze pollution by black carbon in megacities in China, Geophys Res Lett, 43, 2873-2879, 10.1002/2016GL067745, 2016.

Dubovik, O., and King, M. D.: A flexible inversion algorithm for retrieval of aerosol optical properties from Sun and sky radiance measurements, J Geophys Res-Atmos, 105, 20673-20696, Doi 10.1029/2000jd900282, 2000.

Dubovik, O., Sinyuk, A., Lapyonok, T., Holben, B. N., Mishchenko, M., Yang, P., Eck, T. F., Volten, H., Munoz, O., Veihelmann, B., van der Zande, W. J., Leon, J. F., Sorokin, M., and Slutsker, I.: Application of spheroid models to account for aerosol particle nonsphericity in remote sensing of desert dust, J Geophys Res-Atmos, 111, Artn D11208 10.1029/2005jd006619, 2006.

Dyson, L. L.: A heavy rainfall sounding climatology over Gauteng, South Africa, using self-organising maps, Clim Dynam, 45, 3051-3065, 10.1007/s00382-015-2523-3, 2015.

Eck, T. F., Holben, B. N., Dubovik, O., Smirnov, A., Goloub, P., Chen, H. B., Chatenet, B., Gomes, L., Zhang, X. Y., Tsay, S. C., Ji, Q., Giles, D., and Slutsker, I.: Columnar aerosol optical properties at AERONET sites in central eastern Asia and aerosol transport to the tropical mid-Pacific, J Geophys Res-Atmos, 110, Artn D06202 10.1029/2004jd005274, 2005.

Fan, S. J., Wang, B. M., Tesche, M., Engelmann, R., Althausen, A., Liu, J., Zhu, W., Fan, Q., Li, M. H., Ta, N., Song, L. L., and Leong, K. C.: Meteorological conditions and structures of atmospheric boundary layer in October 2004 over Pearl River Delta area, Atmos Environ, 42, 6174-6186, 10.1016/j.atmosenv.2008.01.067, 2008.

Gao, M., Carmichael, G. R., Wang, Y., Saide, P. E., Yu, M., Xin, J., Liu, Z., and Wang, Z.: Modeling study of the 2010 regional haze event in the North China Plain, Atmos Chem Phys, 16, 1673-1691, 10.5194/acp-16-1673-2016, 2016.

Ge, J. M., Su, J., Ackerman, T. P., Fu, Q., Huang, J. P., and Shi, J. S.: Dust aerosol optical properties retrieval and radiative forcing over northwestern China during the 2008 China-US joint field experiment, J Geophys Res-Atmos, 115, Artn D00k12 10.1029/2009jd013263, 2010.

Gibson, P. B., Perkins-Kirkpatrick, S. E., and Renwick, J. A.: Projected changes in synoptic weather patterns over New Zealand examined through self-organizing maps, Int J Climatol, 36, 3934-3948, 10.1002/joc.4604, 2016.

Guinot, B., Roger, J. C., Cachier, H., Wang, P. C., Bai, J. H., and Tong, Y.: Impact of vertical atmospheric structure on Beijing aerosol distribution, Atmos Environ, 40, 5167-5180, 10.1016/j.atmosenv.2006.03.051, 2006.

Atmos. Chem. Phys. Discuss., https://doi.org/10.5194/acp-2017-1046
Manuscript under review for journal Atmos. Chem. Phys.
Discussion started: 13 December 2017

Guo, J. P., Miao, Y. C., Zhang, Y., Liu, H., Li, Z. Q., Zhang, W. C., He, J., Lou, M. Y., Yan, Y., Bian, L. G., and Zhai, P.: The climatology of planetary boundary layer height in China derived from radiosonde and reanalysis data, Atmos Chem Phys, 16, 13309-13319, 10.5194/acp-16-13309-2016, 2016.

Haman, C. L., Couzo, E., Flynn, J. H., Vizuete, W., Heffron, B., and Lefer, B. L.: Relationship between boundary layer heights and growth rates with ground-level ozone in Houston, Texas, J Geophys Res-Atmos, 119, 6230-6245, 10.1002/2013JD020473, 2014.

Han, S. Q., Bian, H., Tie, X. X., Xie, Y. Y., Sun, M. L., and Liu, A. X.: Impact of nocturnal planetary boundary layer on urban air pollutants: Measurements from a 250-m tower over Tianjin, China, J Hazard Mater, 162, 264-269, 10.1016/j.jhazmat.2008.05.056, 2009.

Hu, X. M., Ma, Z. Q., Lin, W. L., Zhang, H. L., Hu, J. L., Wang, Y., Xu, X. B., Fuentes, J. D., and Xue, M.: Impact of the Loess Plateau on the atmospheric boundary layer structure and air quality in the North China Plain: A case study, Sci Total Environ, 499, 228-237, 10.1016/j.scitotenv.2014.08.053, 2014.

Hua, Y., Wang, S., Wang, J., Jiang, J., Zhang, T., Song, Y., Kang, L., Zhou, W., Cai, R., Wu, D., Fan, S., Wang, T., Tang, X., Wei, Q., Sun, F., and Xiao, Z.: Investigating the impact of regional transport on PM2.5 formation using vertical observation during APEC 2014 Summit in Beijing, Atmos Chem Phys, 16, 15451-15460, 10.5194/acp-16-15451-2016, 2016.

Jenner, S. L., and Abiodun, B. J.: The transport of atmospheric sulfur over Cape Town, Atmos Environ, 79, 248-260, 10.1016/j.atmosenv.2013.06.010, 2013.

Jensen, A. A., Thompson, A. M., and Schmidlin, F. J.: Classification of Ascension Island and Natal ozonesondes using self-organizing maps, J Geophys Res-Atmos, 117, Artn D04302
10.1029/2011jd016573, 2012.

Ji, D. S., Wang, Y. S., Wang, L. L., Chen, L. F., Hu, B., Tang, G. Q., Xin, J. Y., Song, T., Wen, T. X., Sun, Y., Pan, Y. P., and Liu, Z. R.: Analysis of heavy pollution episodes in selected cities of northern China, Atmos Environ, 50, 338-348, 10.1016/j.atmosenv.2011.11.053, 2012.

Jia, Y. T., Rahn, K. A., He, K. B., Wen, T. X., and Wang, Y. S.: A novel technique for quantifying the regional component of urban aerosol solely from its sawtooth cycles, J Geophys Res-Atmos, 113, Artn D21309
10.1029/2008jd010389, 2008.

Jiang, N. B., Scorgie, Y., Hart, M., Riley, M. L., Crawford, J., Beggs, P. J., Edwards, G. C., Chang, L. S., Salter, D., and Virgilio, G. D.: Visualising the relationships between synoptic circulation type and air quality in Sydney, a subtropical coastal-basin environment, Int J Climatol, 37, 1211-1228, 10.1002/joc.4770, 2017.

Kajino, M., Ueda, H., Han, Z., Kudo, R., Inomata, Y., and Kaku, H.: Synergy between air pollution and urban meteorological changes through aerosol-radiation-diffusion feedback—A case study of Beijing in January 2013, Atmos Environ, 171, 98-110, https://doi.org/10.1016/j.atmosenv.2017.10.018, 2017.

Katurji, M., Noonan, B., Zawar-Reza, P., Schulmann, T., and Sturman, A.: Characteristics of the Springtime Alpine Valley Atmospheric Boundary Layer Using Self-Organizing Maps, J Appl Meteorol Clim, 54, 2077-2085, 10.1175/Jamc-D-14-0317.1, 2015.

Kohonen, T.: Self-organized information of topologically correct features maps, Biological Cybernetics 43, 59-69, 1982.

Kohonen, T.: Self-organizing maps, 3rd edn. Springer, London, 2001.

Lennard, C., and Hegerl, G.: Relating changes in synoptic circulation to the surface rainfall response using self-organising maps, Clim Dynam, 44, 861-879, 10.1007/s00382-014-2169-6, 2015.

Li, J., Du, H., Wang, Z., Sun, Y., Yang, W., Li, J., Tang, X., and Fu, P.: Rapid formation of a severe regional winter haze episode over a mega-city cluster on the North China Plain, Environ Pollut, 223, 605-615, https://doi.org/10.1016/j.envpol.2017.01.063, 2017a.

Li, J., Sun, J., Zhou, M., Cheng, Z., Li, Q., Cao, X., and Zhang, J.: Observational Analyses of Dramatic Developments of A Severe Air Pollution Event in the Beijing Area, Atmos. Chem. Phys. Discuss., 2017, 1-24, 10.5194/acp-2017-909, 2017b.

Li, Y. R., Ye, C. X., Liu, J., Zhu, Y., Wang, J. X., Tan, Z. Q., Lin, W. L., Zeng, L. M., and Zhu, T.: Observation of regional air

Atmos. Chem. Phys. Discuss., https://doi.org/10.5194/acp-2017-1046
Manuscript under review for journal Atmos. Chem. Phys.
Discussion started: 13 December 2017

Atmospheric Chemistry and Physics
Discussions

pollutant transport between the megacity Beijing and the North China Plain, Atmos Chem Phys, 16, 14265-14283, 10.5194/acp-16-14265-2016, 2016.

Li, Z. Q., Lee, K. H., Wang, Y. S., Xin, J. Y., and Hao, W. M.: First observation-based estimates of cloud-free aerosol radiative forcing across China, J Geophys Res-Atmos, 115, Artn D00k18 10.1029/2009jd013306, 2010.

Liu, Y. G., Weisberg, R. H., and Mooers, C. N. K.: Performance evaluation of the self-organizing map for feature extraction, J Geophys Res-Oceans, 111, Artn C05018 10.1029/2005jc003117, 2006.

Miao, Y., Guo, J., Liu, S., Liu, H., Li, Z., Zhang, W., and Zhai, P.: Classification of summertime synoptic patterns in Beijing and their associations with boundary layer structure affecting aerosol pollution, Atmos Chem Phys, 17, 3097-3110, 10.5194/acp-17-3097-2017, 2017.

Pearce, J. L., Waller, L. A., Chang, H. H., Klein, M., Mulholland, J. A., Sarnat, J. A., Sarnat, S. E., Strickland, M. J., and Tolbert, P. E.: Using self-organizing maps to develop ambient air quality classifications: a time series example, Environ Health-Glob, 13, 10.1186/1476-069X-13-56, 2014.

Platis, A., Altstadter, B., Wehner, B., Wildmann, N., Lampert, A., Hermann, M., Birmili, W., and Bange, J.: An Observational Case Study on the Influence of Atmospheric Boundary-Layer Dynamics on New Particle Formation, Bound-Lay Meteorol, 158, 67-92, 10.1007/s10546-015-0084-y, 2016.

Quan, J. N., Gao, Y., Zhang, Q., Tie, X. X., Cao, J. J., Han, S. Q., Meng, J. W., Chen, P. F., and Zhao, D. L.: Evolution of planetary boundary layer under different weather conditions, and its impact on aerosol concentrations, Particuology, 11, 34-40, 10.1016/j.partic.2012.04.005, 2013.

Salmond, J. A., and McKendry, I. G.: A review of turbulence in the very stable nocturnal boundary layer and its implications for air quality, Progress in Physical Geography, 29, 171-188, 10.1191/0309133305pp442ra, 2005.

Seinfeld, J. H., and Pandis, S. N.: Atmospheric Chemistry and Physics: From Air Pollution to Climate Change 2nd edn (New York: Wiley), 2006.

Stauffer, R. M., Thompson, A. M., and Young, G. S.: Tropospheric ozonesonde profiles at long-term US monitoring sites: 1. A climatology based on self-organizing maps, J Geophys Res-Atmos, 121, 1320-1339, 10.1002/2015JD023641, 2016.

Stull, R. B.: An Introduction to Boundary Layer Meteorology. Kluwer, 1988.

Sun, Y., Song, T., Tang, G. Q., and Wang, Y. S.: The vertical distribution of PM2.5 and boundary-layer structure during summer haze in Beijing, Atmos Environ, 74, 413-421, 10.1016/j.atmosenv.2013.03.011, 2013.

Sun, Y. L., Du, W., Wan, Q. Q., Zhang, Q., Chen, C., Chen, Y., Chen, Z. Y., Fu, P. Q., Wang, Z. F., Gao, Z. Q., and Worsnop, D. R.: Real-Time Characterization of Aerosol Particle Composition above the Urban Canopy in Beijing: Insights into the Interactions between the Atmospheric Boundary Layer and Aerosol Chemistry, Environ Sci Technol, 49, 11340-11347, 10.1021/acs.est.5b02373, 2015.

Tang, G., Zhu, X., Hu, B., Xin, J., Wang, L., Munkel, C., Mao, G., and Wang, Y.: Impact of emission controls on air quality in Beijing during APEC 2014: lidar ceilometer observations, Atmos Chem Phys, 15, 12667-12680, 10.5194/acp-15-12667-2015, 2015.

Tang, G. Q., Zhang, J. Q., Zhu, X. W., Song, T., Munkel, C., Hu, B., Schafer, K., Liu, Z. R., Zhang, J. K., Wang, L. L., Xin, J. Y., Suppan, P., and Wang, Y. S.: Mixing layer height and its implications for air pollution over Beijing, China, Atmos Chem Phys, 16, 2459-2475, 10.5194/acp-16-2459-2016, 2016.

Tong, N. Y. O., Leung, D. Y. C., and Liu, C. H.: A Review on Ozone Evolution and Its Relationship with Boundary Layer Characteristics in Urban Environments, Water Air Soil Poll, 214, 13-36, 10.1007/s11270-010-0438-5, 2011.

Whiteman, C. D., Hoch, S. W., Horel, J. D., and Charland, A.: Relationship between particulate air pollution and meteorological variables in Utah's Salt Lake Valley, Atmos Environ, 94, 742-753, 10.1016/j.atmosenv.2014.06.012, 2014.

Wolf, T., Esau, I., and Reuder, J.: Analysis of the vertical temperature structure in the Bergen valley, Norway, and its connection to pollution episodes, J Geophys Res-Atmos, 119, 10645-10662, 10.1002/2014JD022085, 2014.

Wu, M., Wu, D., Fan, Q., Wang, B. M., Li, H. W., and Fan, S. J.: Observational studies of the meteorological characteristics associated with poor air quality over the Pearl River Delta in China, Atmos Chem Phys, 13, 10755-10766, 10.5194/acp-13-10755-2013, 2013.

Xia, X., Chen, H., and Zhang, W.: Analysis of the dependence of column-integrated aerosol properties on long-range transport of air masses in Beijing, Atmos Environ, 41, 7739-7750, 10.1016/j.atmosenv.2007.06.042, 2007.

Xu, X., Zhao, T., Liu, F., Gong, S. L., Kristovich, D., Lu, C., Guo, Y., Cheng, X., Wang, Y., and Ding, G.: Climate modulation of the Tibetan Plateau on haze in China, Atmos Chem Phys, 16, 1365-1375, 10.5194/acp-16-1365-2016, 2016.

Ye, X. X., Song, Y., Cai, X. H., and Zhang, H. S.: Study on the synoptic flow patterns and boundary layer process of the severe haze events over the North China Plain in January 2013, Atmos Environ, 124, 129-145, 10.1016/j.atmosenv.2015.06.011, 2016.

Yu, X. N., Zhu, B., and Zhang, M. G.: Seasonal variability of aerosol optical properties over Beijing, Atmos Environ, 43, 4095-4101, 10.1016/j.atmosenv.2009.03.061, 2009.

Yu, X. N., Lu, R., Kumar, K. R., Ma, J., Zhang, Q. J., Jiang, Y. L., Kang, N., Yang, S. Y., Wang, J., and Li, M.: Dust aerosol properties and radiative forcing observed in spring during 2001-2014 over urban Beijing, China, Environ Sci Pollut R, 23, 15432-15442, 10.1007/s11356-016-6727-9, 2016.

Yu, X. N., Lu, R., Liu, C., Yuan, L., Shao, Y. X., Zhu, B., and Lei, L.: Seasonal variation of columnar aerosol optical properties and radiative forcing over Beijing, China, Atmos Environ, 166, 340-350, 10.1016/j.atmosenv.2017.07.011, 2017.

Zhang, J. P., Zhu, T., Zhang, Q. H., Li, C. C., Shu, H. L., Ying, Y., Dai, Z. P., Wang, X., Liu, X. Y., Liang, A. M., Shen, H. X., and Yi, B. Q.: The impact of circulation patterns on regional transport pathways and air quality over Beijing and its surroundings, Atmos Chem Phys, 12, 5031-5053, 10.5194/acp-12-5031-2012, 2012a.

Zhang, Q., Ma, X. C., Tie, X. X., Huang, M. Y., and Zhao, C. S.: Vertical distributions of aerosols under different weather conditions: Analysis of in-situ aircraft measurements in Beijing, China, Atmos Environ, 43, 5526-5535, 10.1016/j.atmosenv.2009.05.037, 2009.

Zhang, Y. L., and Cao, F.: Fine particulate matter (PM2.5) in China at a city level, Sci Rep-Uk, 5, Artn 14884 10.1038/Srep14884, 2015.

Zhang, Z. Y., Wang, F. J., Costabile, F., Allegrini, I., Liu, F. L., and Hong, W. M.: Interpretation of ground-level ozone episodes with atmospheric stability index measurement, Environ Sci Pollut R, 19, 3421-3429, 10.1007/s11356-012-0867-3, 2012b.

Zhao, B., Wang, P., Ma, J. Z., Zhu, S., Pozzer, A., and Li, W.: A high-resolution emission inventory of primary pollutants for the Huabei region, China, Atmos Chem Phys, 12, 481-501, 10.5194/acp-12-481-2012, 2012.

Zhao, G., Zhao, C., Kuang, Y., Tao, J., Tan, W., Bian, Y., Li, J., and Li, C.: Impact of aerosol hygroscopic growth on retrieving aerosol extinction coefficient profiles from elastic-backscatter lidar signals, Atmos. Chem. Phys., 17, 12133-12143, 10.5194/acp-17-12133-2017, 2017.

Zhao, X. J., Zhao, P. S., Xu, J., Meng, W., Pu, W. W., Dong, F., He, D., and Shi, Q. F.: Analysis of a winter regional haze event and its formation mechanism in the North China Plain, Atmos Chem Phys, 13, 5685-5696, 10.5194/acp-13-5685-2013, 2013.

Zheng, G. J., Duan, F. K., Su, H., Ma, Y. L., Cheng, Y., Zheng, B., Zhang, Q., Huang, T., Kimoto, T., Chang, D., Poschl, U., Cheng, Y. F., and He, K. B.: Exploring the severe winter haze in Beijing: the impact of synoptic weather, regional transport and heterogeneous reactions, Atmos Chem Phys, 15, 2969-2983, 10.5194/acp-15-2969-2015, 2015.

Zhong, J., Zhang, X., Dong, Y., Wang, Y., Wang, J., Zhang, Y., and Che, H.: Feedback effects of boundary-layer meteorological factors on explosive growth of PM2.5 during winter heavy pollution episodes in Beijing from 2013 to 2016, Atmos. Chem. Phys. Discuss., 2017, 1-25, 10.5194/acp-2017-845, 2017.

Zhu, X. W., Tang, G. Q., Hu, B., Wang, L. L., Xin, J. Y., Zhang, J. K., Liu, Z. R., Munkel, C., and Wang, Y. S.: Regional pollution and its formation mechanism over North China Plain: A case study with ceilometer observations and model simulations, J Geophys Res-Atmos, 121, 14574-14588, 10.1002/2016JD025730, 2016.

Zou, J., Sun, J. N., Ding, A. J., Wang, M. H., Guo, W. D., and Fu, C. B.: Observation-based estimation of aerosol-induced reduction of planetary boundary layer height, Adv Atmos Sci, 34, 1057-1068, 10.1007/s00376-016-6259-8, 2017.

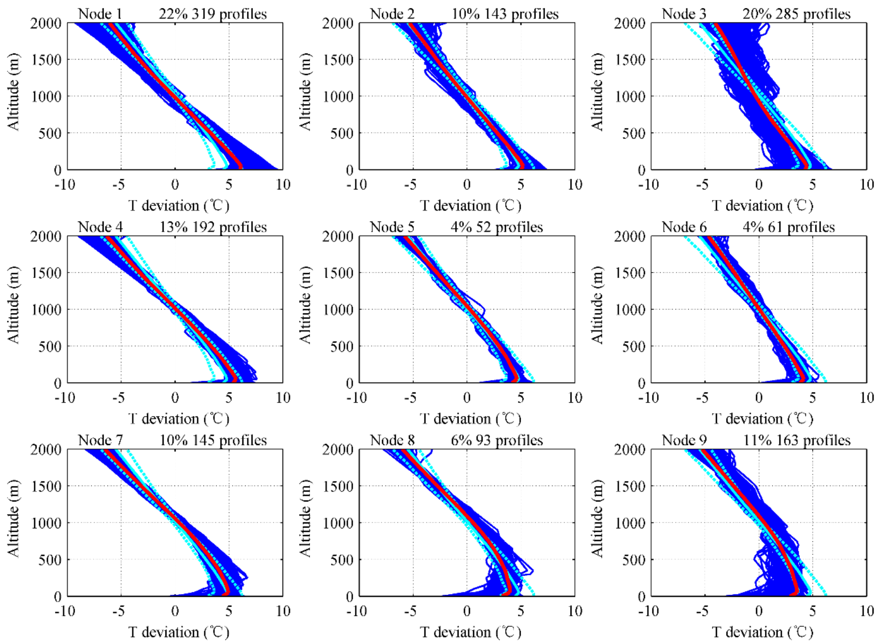

Figure 1. The 3 × 3 SOM output for radiosonde-based temperature (T) deviation profiles observed at the Beijing Observatory. SOM nodes are shown in red, with the corresponding individual profiles in dark blue. For reference, the overall average temperature profile and 25th and 75th percentile profiles are shown in cyan. The top-right shows the occurrence cases and frequency of each SOM node.

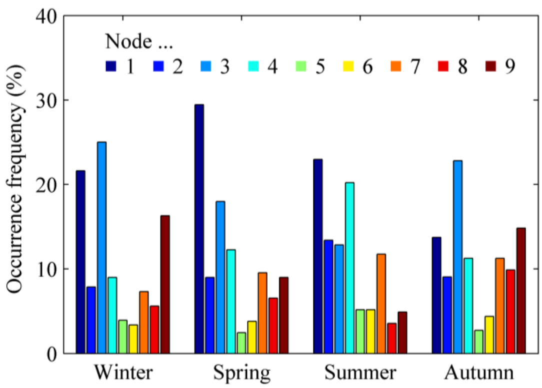

Figure 2. Seasonality of SOM nodes shown as the relative frequency of seasons within each SOM node. Winter (DJF); Spring (MAM); Summer (JJA); Autumn (SON).

Atmos. Chem. Phys. Discuss., https://doi.org/10.5194/acp-2017-1046
Manuscript under review for journal Atmos. Chem. Phys.
Discussion started: 13 December 2017

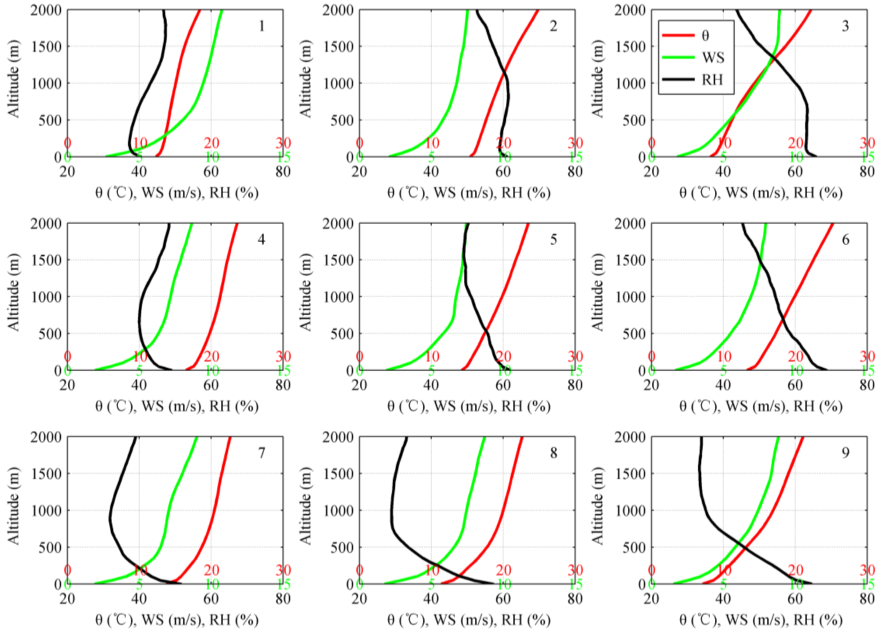

Figure 3. Profiles of average potential temperature (θ), wind speed (WS) and relative humidity (RH) corresponding to each SOM node at the Beijing Observatory. The red, green and black labels of the horizontal axis correspond to θ, WS and RH, respectively.

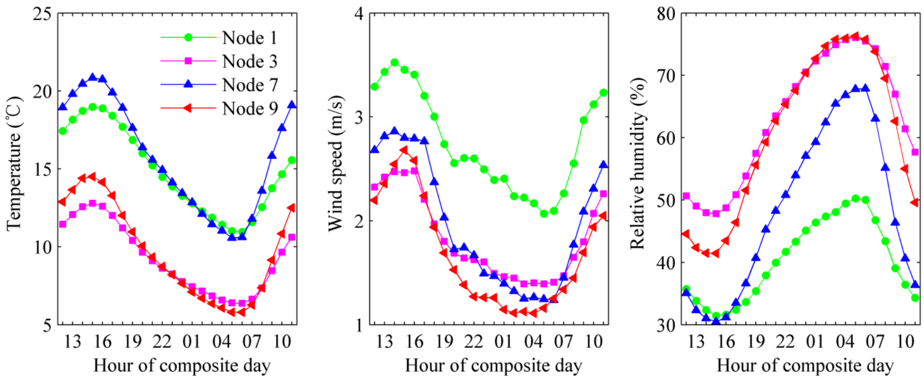

Figure 4. Hourly mean diurnal composites of temperature, wind speed and relative humidity in Beijing corresponding to SOM nodes 1, 3, 7 and 9.

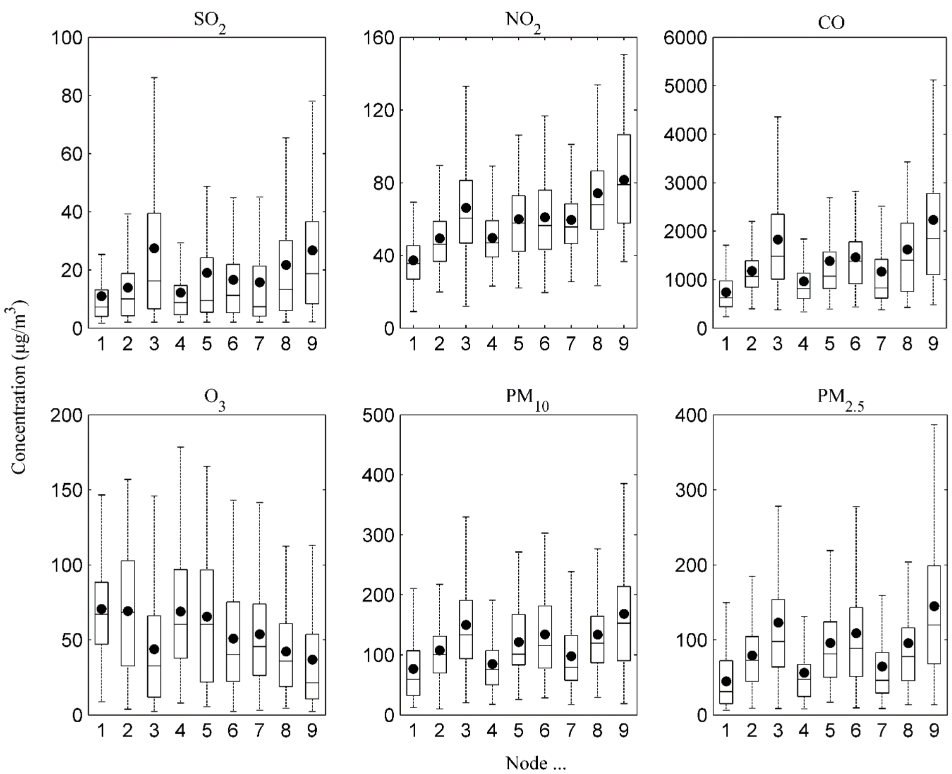

Figure 5. Daily pollutant concentrations in Beijing corresponding to each SOM node. The solid dots denote the mean. The box and whisker plot presents the median, the first and third quartiles, and the 5th and 95th percentiles, respectively.

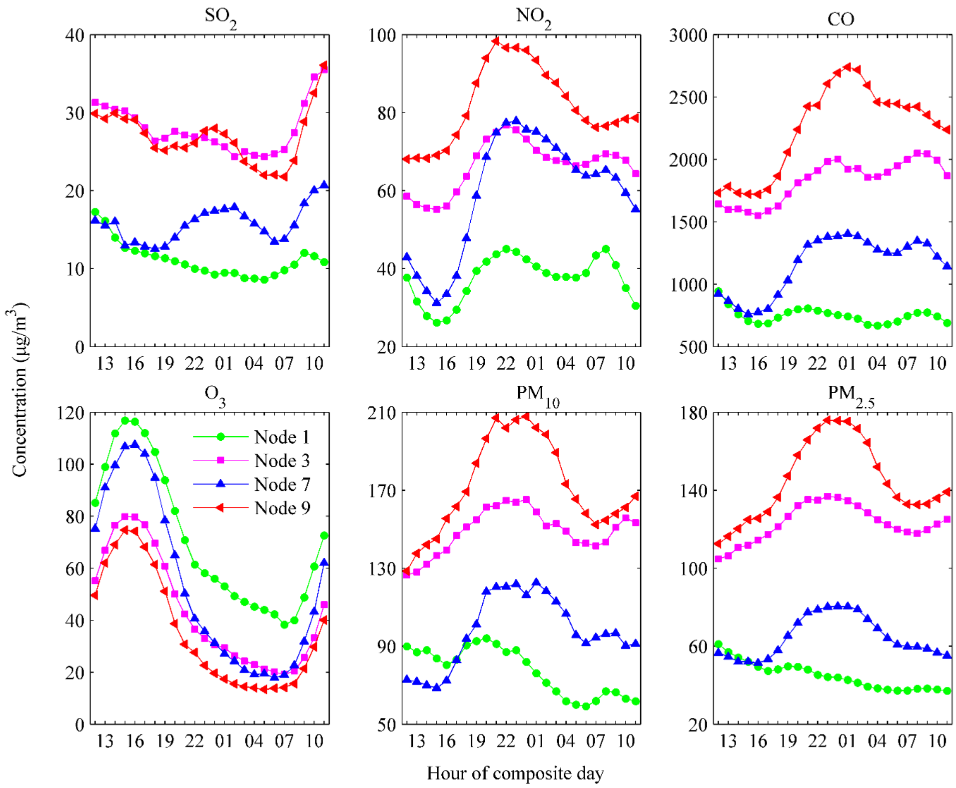

Figure 6. Composite diurnal variations of air pollutants in Beijing corresponding to SOM nodes 1, 3, 7 and 9.

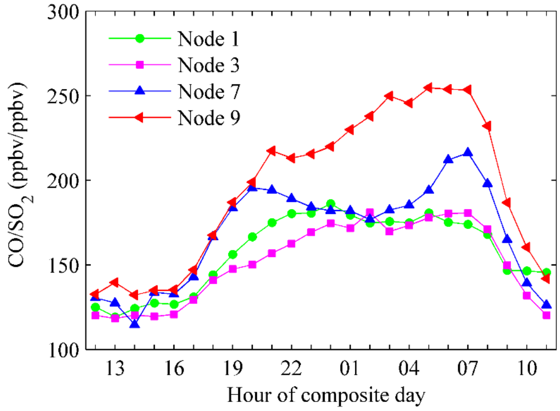

Figure 7. Composite diurnal variations of CO/SO_2 ratios in Beijing corresponding to SOM nodes 1, 3, 7 and 9.

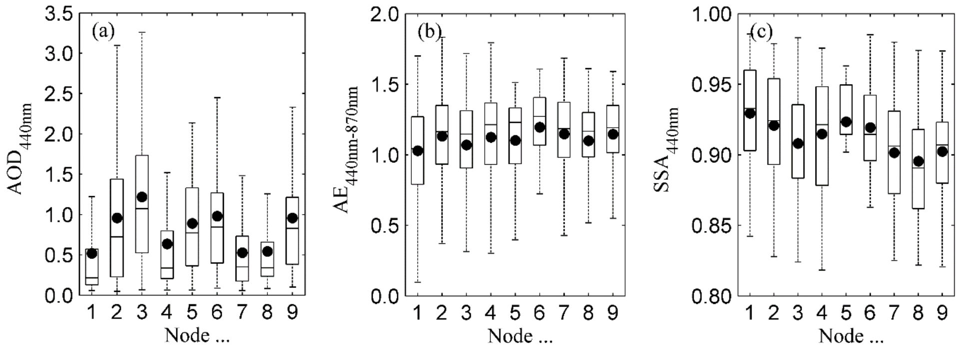

Figure 8. (a) Aerosol optical depth (AOD_{440nm}), (b) Ångström exponent ($AE_{440nm-870nm}$) and (c) single scattering albedo (SSA_{440nm}) over Beijing and corresponding to each SOM node. The solid dots denote the mean. The box and whisker plot presents the median, the first and third quartiles, and the 5th and 95th percentiles, respectively.

Atmos. Chem. Phys. Discuss., https://doi.org/10.5194/acp-2017-1046
Manuscript under review for journal Atmos. Chem. Phys.
Discussion started: 13 December 2017

Atmospheric Chemistry and Physics
Discussions
Open Access

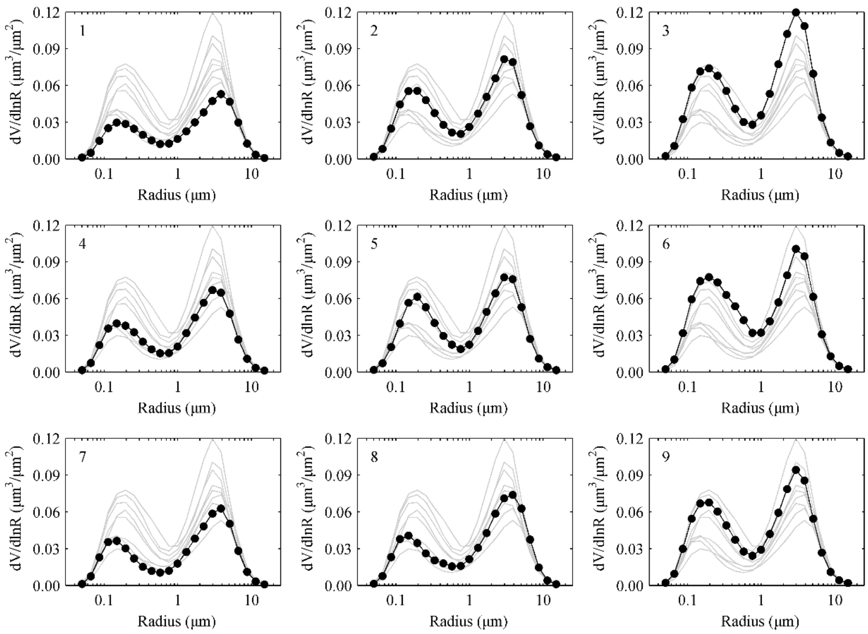

Figure 9. Mean volume particle size distribution over Beijing corresponding to each SOM node. The average volume particle size distribution for each node is shown by the gray line and is repeated on each plot for comparison. The size distribution for each type is highlighted in the black dotted line on the respective plot.

Atmos. Chem. Phys. Discuss., https://doi.org/10.5194/acp-2017-1046
Manuscript under review for journal Atmos. Chem. Phys.
Discussion started: 13 December 2017

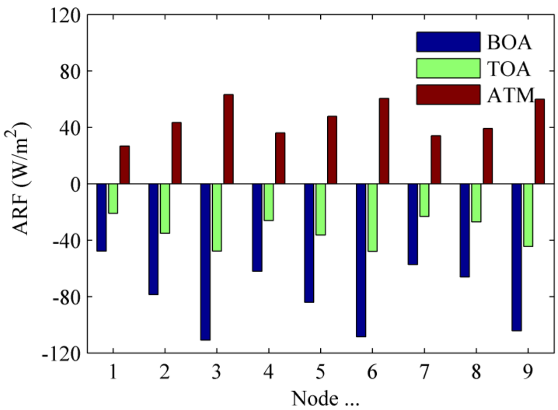

Figure 10. Aerosol radiative forcing (ARF) at the surface (BOA), top of atmosphere (TOA), and within the atmosphere (ATM) over Beijing and corresponding to each SOM node.

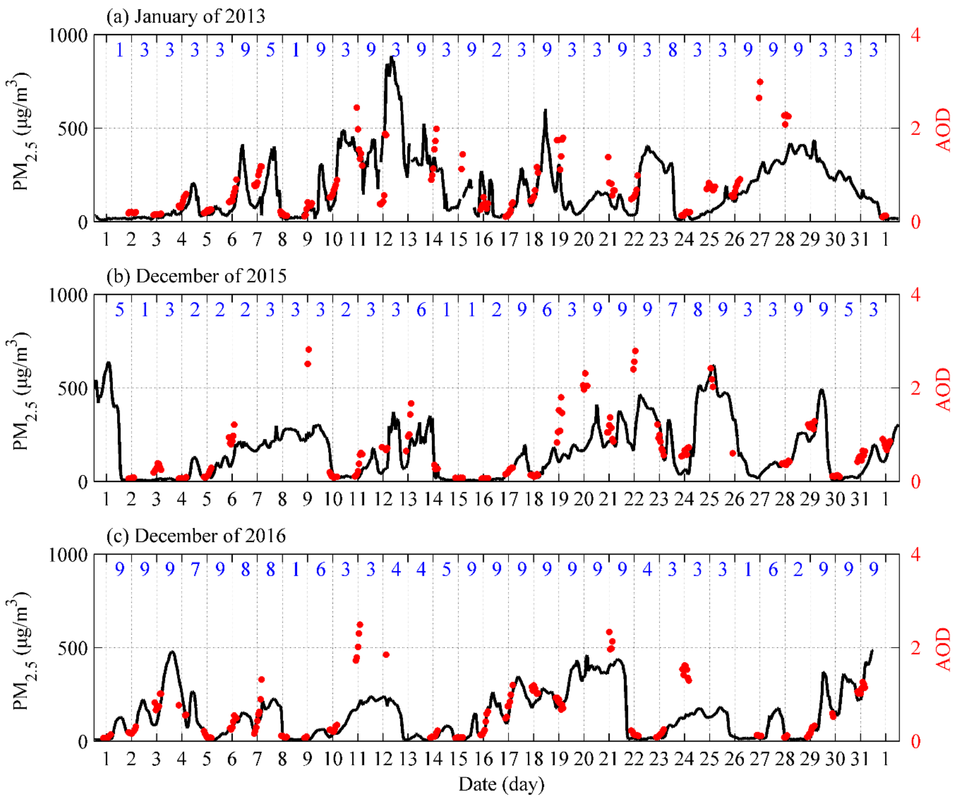

Figure 11. Time series of hourly $PM_{2.5}$ and AOD_{440nm} in (a) January of 2013, (b) December of 2015, and (c) December of 2016. The daily SOM nodes (i.e., ABL types) are shown at the top of each plot (blue numbers).

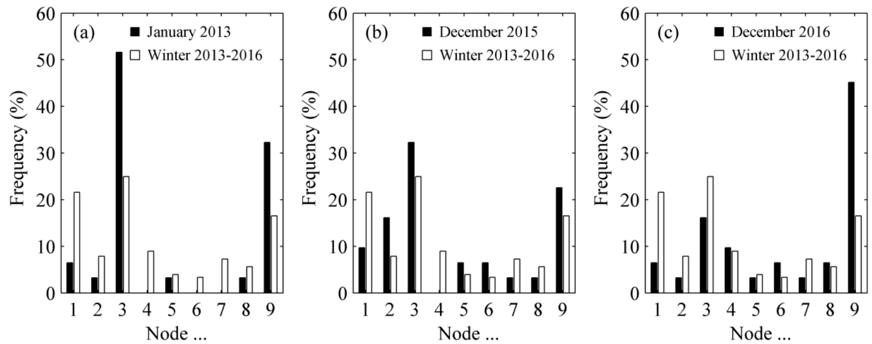

Figure 12. Occurrence frequency of the SOM nodes during (a) January 2013, (b) December 2015, and (c) December 2016.

Atmos. Chem. Phys. Discuss., https://doi.org/10.5194/acp-2017-1046
Manuscript under review for journal Atmos. Chem. Phys.
Discussion started: 13 December 2017

Node …	Effective radius (μm)			Volume concentration ($\mu m^3/\mu m^2$)			*Vf*/*Vt*
	R_{eff}-T	R_{eff}-F	R_{eff}-C	VolCon-T	VolCon-F	VolCon-C	
1	0.54	0.14	2.46	0.13	0.05	0.09	0.31
2	0.41	0.16	2.42	0.21	0.09	0.12	0.42
3	0.45	0.16	2.30	0.30	0.12	0.18	0.41
4	0.45	0.15	2.38	0.17	0.06	0.11	0.36
5	0.47	0.17	2.44	0.21	0.09	0.12	0.41
6	0.38	0.17	2.33	0.28	0.14	0.14	0.45
7	0.42	0.14	2.37	0.15	0.05	0.10	0.34
8	0.44	0.14	2.32	0.18	0.06	0.12	0.35
9	0.38	0.16	2.25	0.25	0.11	0.14	0.43

Table 1. Statistical parameters of aerosol particle size distribution corresponding to each SOM node. VolCon is the volume concentration; R_{eff} the effective radius; *Vf*/*Vt* denotes the fine-mode volume fraction. T, F, and C represent the total, fine-, and coarse-mode particles.